Available online at www.sciencedirect.com
ScienceDirect
Journal of Photochemistry and Photobiology A: Chemistry 194 (2008) 181–188
Journal of Photochemistry and Photobiology A:Chemistry
www.elsevier.com/locate/jphotochem

A comparative study into the photocatalytic properties of thin mesoporous layers of TiO_2 with controlled mesoporosity

Jessica Tschirch [a,b,*], Detlef Bahnemann [a], Michael Wark [b], Jiří Rathouský [c]

[a] *Institute of Technical Chemistry, Leibniz University Hannover, Callinstr. 3, D-30167 Hannover, Germany*
[b] *Institute of Physical Chemistry and Electrochemistry, Leibniz University of Hanover, Callin Str. 3A, D-30167 Hannover, Germany*
[c] *J. Heyrovský Institute of Physical Chemistry of ASCR, v.v.i., Dolejškova 8, CZ-18223 Prague 8, Czech Republic*

Received 24 April 2007; received in revised form 31 July 2007; accepted 4 August 2007
Available online 10 August 2007

Abstract

Mesoporous films of TiO_2 were prepared by a sol–gel procedure using a Pluronic® block copolymer and the dip-coating technique. The film thickness was controlled by changing the film withdrawal rate and by repetitive coatings. The amount of dye molecules adsorbed onto the mesoporous film depends on the dye properties, with thionine and methylene blue being more strongly adsorbed than rhodamine B, methyl orange and methyl red. The photocatalytic efficiency of the degradation of these dyes strongly depends on their respective degradation mechanism. It was found that the optimum efficiency is achieved when the target molecule is adsorbed only to some extent thus enabling its decomposition directly by the attack of holes. On the other hand, secondary oxidizing species such as $O_2^{\bullet -}$ and $HO_2^{\bullet}$ but most likely even $OH^{\bullet}$ play a crucial role in the oxidation mechanism, which is particularly evident in the case of methylene red. Higher concentrations of adsorbed species to be degraded may even be detrimental as found when thionine was employed as the model compound.

Keywords: Mesoporous films; Film thickness; TiO_2; Dye adsorption; Photocatalytic degradation

1. Introduction

Due to a number of excellent properties, such as transparency, uniform and organized mesoporosity, complete accessibility of the large inner surface area and a suitable morphology in comparison with powdered materials, ordered mesoporous films of TiO_2 are promising candidates for applications in, e.g., photocatalysis, solar cells, sensors and displays. In recent years, a generalized sol–gel procedure for the preparation of large-pore mesoporous metal oxide films has been developed, based on a mechanism that combines evaporation-induced self-assembly (EISA) of a block copolymer with complexation of molecular inorganic species enabling the preparation of mesoporous films with good mechanical, optical and transport properties [1,2]. Due to the removal of the structure-directing polymer by thermal treatment or extraction, the organic–inorganic mesophase is transformed into a mesoporous solid with controlled porosity. The original EISA method has been improved by precise control of film preparation conditions, variation of the composition of the reaction mixture, introduction of different types of molecular metal oxide precursors and of different polymer templates [3–11].

Generally, research on the metal oxide films with controlled mesoporosity mostly concentrates on the preparative aspects, while the functional properties of these materials have been at the most only partially explored and understood. Recently, several reports have been published dealing with photocatalytic properties of mesoporous films of TiO_2. In the liquid phase the photocatalytic decomposition of methylene blue [12–14], methyl orange [15], 4-chlorophenol [16], in the solid phase of stearic [16] and lauric acids [14] and of methyl stearate [17], and in the gas phase of toluene [18] and acetone [19] have been tested. Highly crystalline mesoporous TiO_2 films have been shown to be active also in water photolysis [20]. Finally, mesoporous films partially covered with platinum nanoparticles have been found effective in the destruction of Micrococcus lylae cells [21].

* Corresponding author at: Institute of Technical Chemistry, Leibniz University Hannover, Callinstr. 3, D-30167 Hannover, Germany. Tel.: +49 5117622773; fax: +49 5117622774.
E-mail addresses: Tschirch@iftc.uni-hannover.de (J. Tschirch), Bahnemann@iftc.uni-hannover.de (D. Bahnemann), michael.wark@pci.uni-hannover.de (M. Wark), jiri.rathousky@jh-inst.cas.cz (J. Rathouský).

1010-6030/$ – see front matter © 2007 Elsevier B.V. All rights reserved.
doi:10.1016/j.jphotochem.2007.08.005

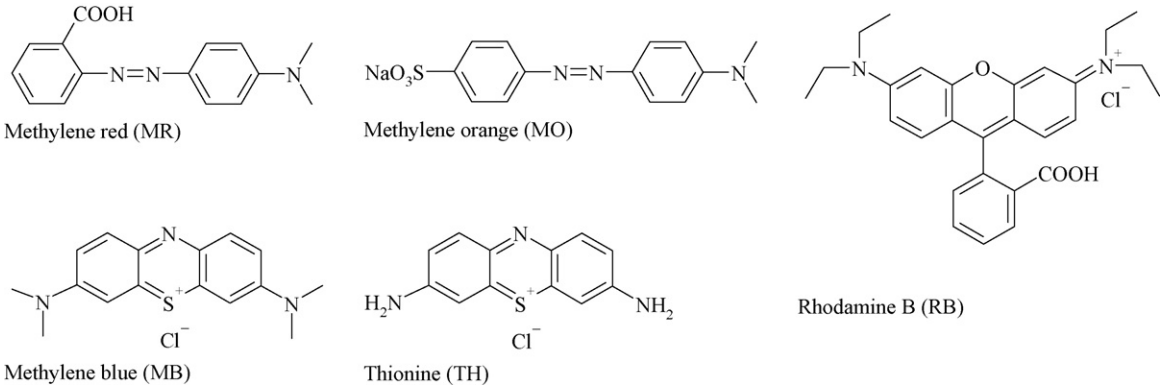

Scheme 1. Chemical formulas showing the structures of the tested dye molecules.

Up to now, however, no comparative study into the photocatalytic performance of such mesoporous films of TiO_2 has been performed, encompassing a series of different model compounds, the degradation mechanisms of which differ substantially. Therefore, it is the main aim of the present study to analyse the activity of mesoporous films of TiO_2 for the photocatalytic decomposition of such a series of selected compounds that are known to be degraded following significantly different mechanisms. Such an analysis should enable to reveal strong and weak features of this type of photocatalyst and should suggest the most suitable fields of its application.

2. Experimental

2.1. Preparation and characterization of mesoporous titania films

Mesoporous titania films were prepared according to the procedure given in Ref. [22], which yields films with a cubic mesostructure. In particular, 16.8 g of titanium (IV) tetraethoxide were dissolved in 12.8 g of concentrated HCl at room temperature under vigorous stirring. After 5 min, a solution of 4 g of Pluronic P123 (BASF) in 48 g of ethanol was added. The resulting solution was subsequently aged at 8 °C for 10 min under stirring before the films were dip-coated onto glass slides at a withdrawal rate of 0.5 or 1 mm/s (designation of the films T0.5 and T1, respectively). Then the films were aged at 8 °C overnight, calcined at 400 °C (achieved at a rate of 1 K/min) for 4 h to remove the block copolymer species. In order to obtain thicker films the dip-coating process was repeated at withdrawal rates of 0.5 or 1 mm/s for several times. Between individual dip-coating steps the films were either calcined or just dried at ambient temperature (designation T2 × 1c and T2 × 1d for a film coated twice at a rate of 1 mm/s with and without intervening calcination steps, respectively).

Morphological parameters of the films were obtained by combining several experimental techniques. The details of the surface texture were provided by high-resolution scanning electron microscopy using a JEM-6700F Jeol apparatus. The film thickness was measured by profilometry using a Sloan Dektak 3030ST. Texture parameters of the films were determined from adsorption isotherms of Kr at 77 K obtained using an ASAP 2010 apparatus (Micromeritics).

The optical properties of the mesoporous TiO_2 films were determined from UV–vis absorption spectra obtained employing a Perkin-Elmer Lambda 19 spectrometer. Interference patterns superimposed on the absorption spectra provided an independent method for the assessment of the film thickness.

2.2. Selection of test substances

Major attention was devoted to the selection of suitable test compounds. In the liquid phase, the degradation of different dyes was studied, while the decomposition of methyl stearate was analyzed in the solid phase.

Three different types of organic dyes with different water solubility were selected: methylene blue (MB) and thionine (TH) as typical heteropolyaromatic compounds; methyl red (MR) and methyl orange (MO) as azo-compounds; and rhodamine B (RB) as a fluorescent pigment (Scheme 1). The photocatalytic decomposition of methylene blue has been reported to be an oxidative process [23–26]. At first, the adsorbed molecules of this dye react with photogenerated holes, h^+, to form the dye radical cation $MB^{\bullet+}$, which by the action of O_2 is converted to $MBOO^{\bullet+}$. The latter peroxy radical further reacts to thionine and finally, in a series of photocatalytic reaction steps, via the intermediates aniline, 4-nitroaniline and acetic acid to water, inorganic acids and CO_2. Indeed, thionine is often detected as an early intermediate during the photocatalytic degradation of methylene blue. For both, methylene blue and thionine, holes, h^+, are directly involved as the active oxidizing species as these dyes are strongly adsorbed onto the photocatalyst's surface (see below).

As both azo-dyes, especially methyl orange, as well as rhodamine B are adsorbed at the TiO_2 surface to a much smaller extent (see below), a direct transfer of holes is less likely. For azo-dyes, the main oxidative species are proposed to be surface bound hydroxyl radicals formed due to the oxidation of water molecules by h^+, but it can also be envisaged that the reductively formed superoxide radicals $O_2^{\bullet-}$ or their protonated form $HO_2^{\bullet}$ contribute to the overall decomposition of these molecules. It has been suggested that the adsorbed dye molecules are initially cleaved in the vicinity of the azo-bond, while the resulting frag-

ments are further oxidized yielding compounds of progressively lower molecular weight and, eventually, CO_2 and inorganic ions [26].

In aqueous solution rhodamine B undergoes a photolytic *N*-de-ethylation accompanied by acetaldehyde formation. This photochemical reaction takes place mainly by direct light absorption of the adsorbed dye molecules and to a lesser extent by the intermediate photoexcitation of the photocatalyst. However, light absorption of dissolved dye molecules practically does not occur. Therefore a sufficient amount of adsorbed dye is needed, which renders mesoporous films of TiO_2 with large and perfectly accessible surface area promising photocatalysts for rhodamine B degradation [27].

For stearic acid, zero-order kinetics for the decomposition reaction providing CO_2 and water have been reported and are usually attributed to the complete coverage of the titania photocatalytic active sites by stearic acid molecules [28]. The overall photocatalytic degradation process has been summarized as follows:

$$C_{17}H_{35}COOH + 26O_2 \xrightarrow{TiO_2, h\nu} 18CO_2 + 18H_2O.$$

In the present study, stearic acid methyl ester (in short: methylstearate) was employed as model compound being present in the solid state and exhibiting no light-absorbing properties. While the initial photocatalytic oxidation step for stearic acid is known to be a Photo-Kolbe decarboxylation followed by the subsequent oxidation of the remaining fatty acid chain, the methyl stearate molecule is attacked by the photogenerated holes in a more or less stochastic way. The latter mechanism has the advantage that due to an unchanged volatility of the initial oxidation products the chances of volatilization phenomena mimicking the photocatalytic degradation will be rather limited.

Because of its importance for any photocatalytic reaction in the liquid phase (but also for most reactions in the gas phase), the degree of adsorption of the dissolved dye molecules onto the surface of the mesoporous titania films was measured. The amount of adsorbed dye was determined from its absorption spectra measured before and after the adsorption process using a Cary 4000 UV–vis spectrophotometer (Varian).

2.3. The photocatalytic tests

The photocatalytic decomposition tests of the dyes were performed as follows [29]. At first, each mesoporous titania film was rinsed with ethanol and afterwards with purified water, followed by drying at ambient temperature for 24 h. After cleaning the samples were irradiated with UV(A) light (λ_{max} = 350 nm, 1 mW/cm^2) for 24 h to decompose possibly remaining organic contaminants by photocatalytic oxidation. A cylindrically shaped glass cell with an inner diameter of 1.65 cm and a height of 4 cm with flat and smooth bottom was attached to each mesoporous titania film using silicon glue. The concentrations of the dye adsorption and test solutions were 0.02 and 0.01 mmol/L, respectively. Six milliliters of the dye adsorption solution was poured into the test cell and the dye was adsorbed in the dark for 12 h. If the remaining concentration of the dye in the solution was larger than that of the test solution, the adsorption was considered to be complete. Otherwise, the procedure was repeated for another 12 h employing fresh adsorption solution. After the adsorption process of the dye was complete, the adsorption solution was replaced by the test solution and the sample was irradiated with 1 mW/cm^2 UV(A) light (20 W UV tube, Eurolite, λ_{max} = 350 nm). The decomposition rate of the dye under the UV(A) light irradiation was determined by measuring its absorption spectrum using a Cary 4000 UV–vis spectrophotometer (Varian) at regular intervals (e.g., every 30 min). The photonic efficiency was calculated as the ratio of the decomposition rate and the flux of incoming UV(A) photons (calculated for the mean wavelength of 350 nm from the employed light intensity of 1 mW/cm^2). As a blank sample, a mesoporous film of SiO_2 with comparable textural properties was used.

For the solid phase tests, a thin film of methyl stearate was coated onto a surface area of the titania film being 4 cm × 2.5 cm in size by evenly spreading 0.5 mL of a 5 mM solution of methyl stearate in *n*-hexane. After an illumination for 24 h (1.5 mW/cm^2, λ_{max} = 350 nm), the remaining methyl stearate film was washed from the surface employing 5 mL *n*-hexane. The concentration of methyl stearate was measured by gas chromatography (Carlo Erba instruments HRGC 500, Column: MN Permabond OV-1-DF-0.25, detector: FID).

3. Results and discussion

3.1. Characteristic properties of mesoporous films of TiO_2

SEM images of the film T1 show a very smooth, uniform porous film structure with the pores being less than 10 nm in size and a pore wall thickness of about 5 nm (Fig. 1). In the dark-field TEM images some small crystals of TiO_2 are clearly recognizable as bright spots (Fig. 2). The selected area electron diffractogram exhibits diffuse rings with few spots evincing thus the presence of very small TiO_2 nanocrystals embedded within an amorphous matrix.

The X-ray diffractograms of all films are almost identical with a broad reflection at ca 25° 2θ, which is indicative for the presence of small particles of anatase, the particle diameters of which are determined to be 5–6 nm as calculated by the Scherrer equation.

Fig. 3 shows the adsorption isotherms of Kr at 77 K for the mesoporous titania films T1 and T2, which have been synthesized with dip-coating withdrawal rates of 1 and 2 mm/s, respectively. The corresponding texture data are given in Table 1. Both isotherms are of type IV characterized by a broad hysteresis loop, which proves the presence of mesopores within the films. The steep adsorption and desorption branches indicate that the films possess a narrow pore size distribution.

3.2. Variation of the film thickness

As the thickness of the films is expected to have a major influence on their photocatalytic performance, several experimental possibilities to obtain a well-determined film thickness variation have been studied. First, the film thickness depends on the rate of film withdrawal from the coating solution. For New-

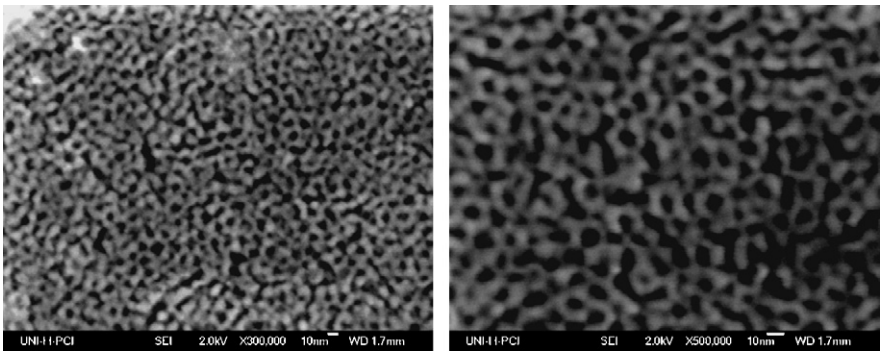

Fig. 1. SEM images of the film T1 coated at a withdrawal rate of 1 mm/s in the dip-coating process.

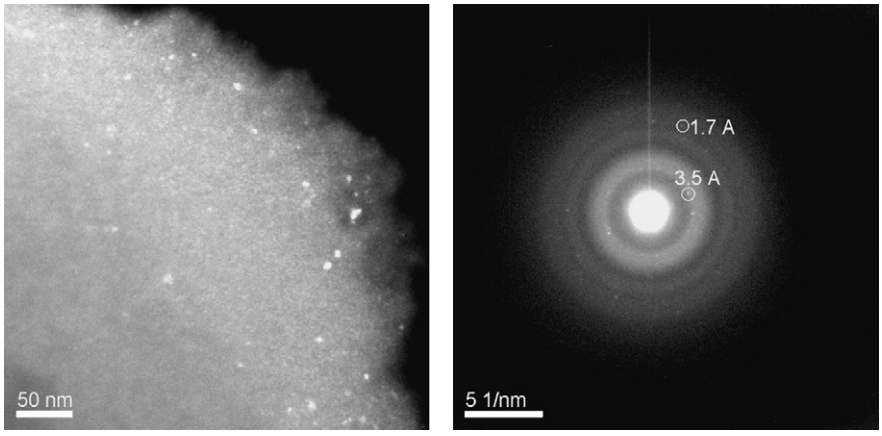

Fig. 2. Left: Dark-field TEM image of film T1, right: selected area electron diffraction pattern of film T1.

ton liquids the film thickness can be calculated according to the Landau–Levich equation:

$$h = 0.94\frac{(\eta v)^{2/3}}{\gamma_{LV}^{1/6}(\rho g)^{1/2}}$$

where h is the film thickness, v the withdrawal rate, η the viscosity of the coating solution and γ_{LV} is the surface tension. Fig. 4 shows that the experimental values are slightly smaller in comparison with those calculated employing the above formula, however, the agreement between predicted and measured values is reasonable. The smaller experimental thickness is clearly due to the contraction of the films during the calcination process. Moreover, a perfect fulfillment of the model assumption cannot be expected for mesoporous films as, e.g., the coating solution is likely to possess non-Newtonian properties due to the presence of the templating block-co-polymer, etc.

Nevertheless, the results shown in Fig. 4 clearly demonstrate that the film thickness can indeed be controlled to a considerable extent by changing the rate of the film withdrawal. As, however, the mechanical properties of thicker films drawn at high withdrawal rates are often not satisfactory, due to insufficient adhesion to the glass support, formation of cracks, etc., the repeated coating method also has been tested here. Two alternative techniques were used, namely, repeated coating with

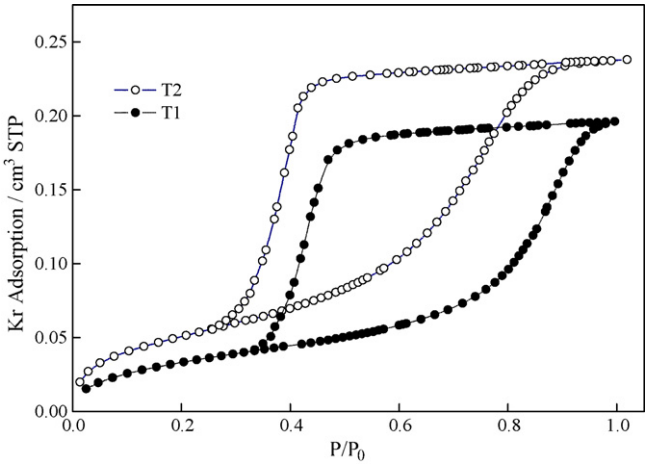

Fig. 3. Adsorption isotherms of Kr at 77 K for films T1 and T2 (compare Table 1).

Table 1
Texture parameters of mesoporous films calculated from adsorption isotherms of Kr at 77 K

Sample	S_{spec} ($cm^2\ cm^{-2}$)	V_{limit} ($\times 10^6\ cm^3\ cm^{-2}$)	D_{ave} (nm)
T1	87	9.7	6.4
T2	136	10.5	4.9
T0.5	33	6.5	7.9
T2 × 0.5c	74	11.1	6.1
T4 × 0.5c	125	16.8	5.4

S_{spec}, specific surface area/1 cm^2 of the support, V_{limit}, pore volume at $P/P_0 \rightarrow 1/cm^2$ of the support; D_{ave}, average pore size.

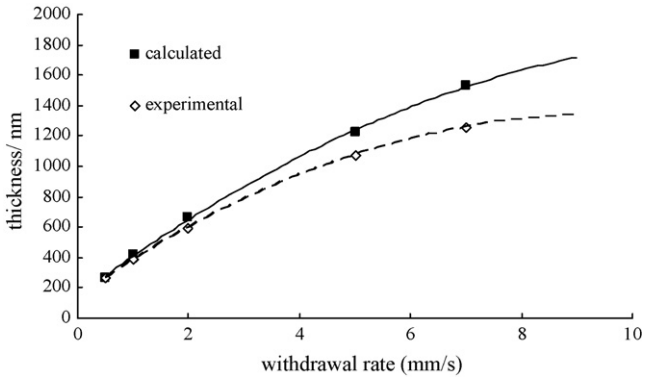

Fig. 4. Dependence of the film thickness on the withdrawal rate during the dip-coating process.

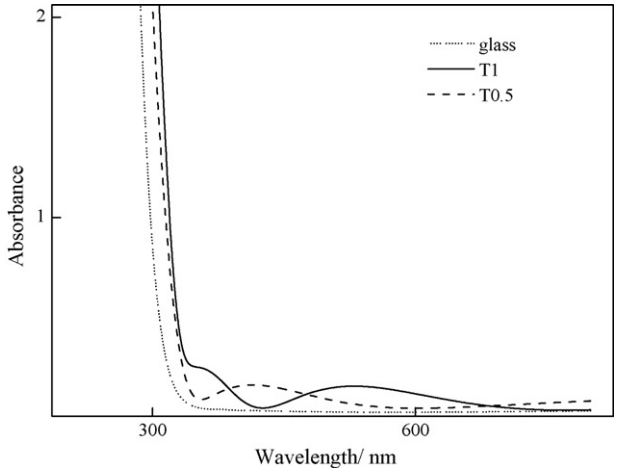

Fig. 6. Transmission UV–vis spectra of the mesoporous films T1 and T0.5.

intervening drying at ambient temperature or intervening calcination, respectively. Generally, it has been found that repeated coating with drying at room temperature is of course much simpler and enables to form thicker films, however, no clear dependence between the number of the coating cycles and the film thickness could be found. The repeated coating with intervening calcination provides films, whose pore size distribution of which is somewhat wider than that of one-step deposited films (compare Fig. 3), as indicated by less steep adsorption and desorption branches in the Kr adsorption isotherms (Fig. 5). However, the thicknesses as well as the texture parameters, such as surface area and pore volume, of these multiple calcined films depend practically linearly on the number of coating cycles (Table 1). This technique is, unfortunately, much more experimentally demanding.

From the measured film thickness (Fig. 4) and the number of interference fringes determined from the UV–vis absorption spectra (Fig. 6), the index of refraction for the mesoporous films can be calculated according to Ref. [30]. For the film drawn at 1 mm/s, the refractive index was calculated to be 2.09. As a mesoporous film consists of anatase pore walls and voids filled with air, such an index of refraction is an effective value and should be given as a volume-weighted average $n_{\text{eff}} = \sqrt{(n_{\text{air}}^2 f + n_{\text{anatase}}^2(1-f))}$ [30], where f is the porosity and n is the respective index of refraction. This formula provides a porosity of 37% for film T1, which is only slightly larger than that determined from the Kr adsorption experiment (30%).

In the UV–vis spectra of the films some shifts of the absorption edge in dependence on the film thickness are also worth to be noted. While the initial inspection of the presented data suggests a slight but clearly discernible red shift of the absorption edge with increasing film thickness, this can simply be explained by the higher absorptivity of the thicker film containing more TiO_2 anatase crystals. Thus, the spectral features are a consequence of Beer's law and not of any quantum-size effect caused by differently sized nanocrystals. As a matter of fact, it is well known that TiO_2 nanocrystals only exhibit quantum-size effects leading to spectral blue-shifts at particle diameters below 2.5 nm, i.e., in a size regime considerably smaller than that of the 5–6 nm particles detected in the walls of the mesoporous films in the present work [31].

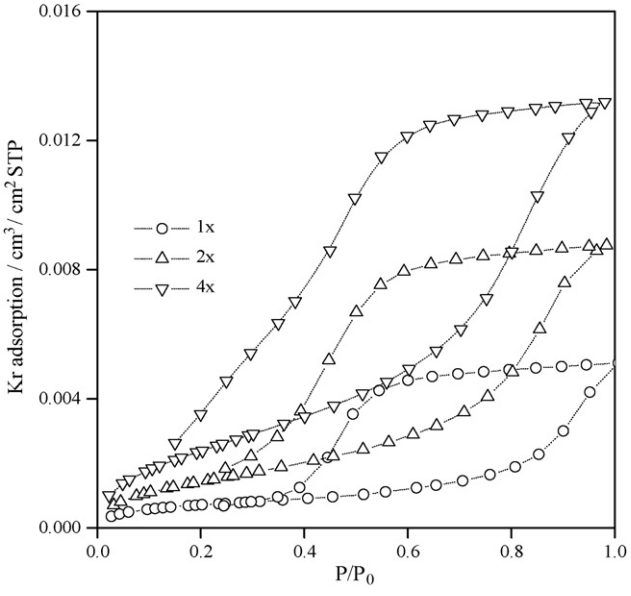

Fig. 5. Adsorption isotherms of Kr on films drawn at 0.5 mm/s once, twice, and four times. Films were calcined between the individual coating steps.

3.3. Dye adsorption

The amount of dye molecules adsorbed onto the mesoporous TiO_2 films strongly depends on the dye properties, provided that other conditions are kept identical (Fig. 7). The equilibrium amount adsorbed per unit surface area of the film T1 is much higher for TH and MB than for the other dyes, achieving 1.36×10^{-10} and 8.7×10^{-11} mol/cm^2, respectively. The adsorption coefficient K can be calculated by the following equation:

$$K = \frac{c_{\text{adsorbed}}}{c_{\text{total}}}$$

Taking $c_{\text{total}} = 0.01$ mM for TH an adsorption coefficient of $K = 1.4$ is calculated being considerably higher than $K = 0.6$ for MB. For the other three dyes the adsorption coefficients are by

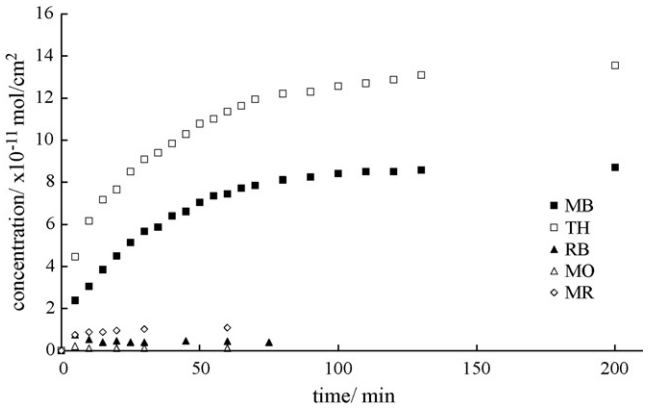

Fig. 7. Adsorption of different dyes on the film T1 (λ_{max} = 664 nm, c = 0.01 mM).

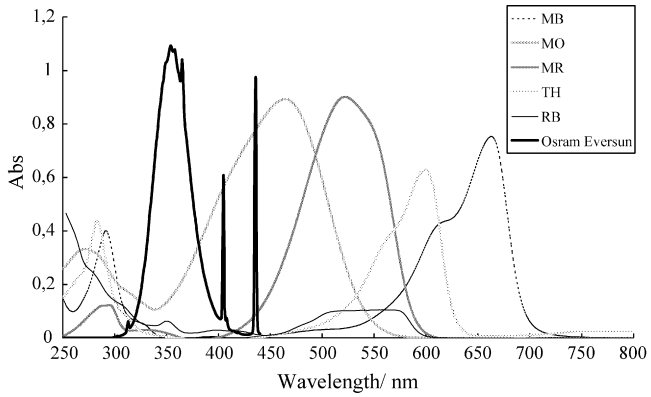

Fig. 8. Absorption spectra showing the absorbance of the different dyes and emission spectrum of the illumination light source (Osram Eversun).

at least one order of magnitude smaller, i.e., only 0.06 for MR, 0.02 for RB and 0.005 for MO. A reasonable explanation for the strong adsorption of TH and MB can be found in the presence of sulfur-centered cations in the heterocycles of these dyes, which strongly interact with the surface-bound OH groups of the TiO_2 films (in particular, when the latter are deprotonated and thus negatively charged above the pH_{zpc}). On the other hand, both MR and RB contain carboxylic groups, whose interaction with the surface is apparently much weaker. This can also be readily explained by an electrostatic model. While the carboxyl groups of the dyes are protonated at acidic pH-values, i.e., where the TiO_2 surface is predominantly positively charged, they are negatively charged in the alkaline pH regime where the TiO_2 surface is also negatively charged resulting in an overall repulsion of the dye molecules. Moreover, the large molecular size of RB leading to higher hydrophobicity further limits its adsorption (its solubility in water is only 0.0001 g/L at 25 °C). Finally, the practically negligible adsorption of MO is due to the absence of suitable polar or charged groups in its molecular structure [32].

The equilibrium adsorption of MB on the film T1 corresponds to 0.575×10^{14} mol/cm^2. As the surface area occupied by a molecule of MB was calculated to be about 0.615 nm^2 [33], the monolayer on an area of 1 cm^2 consists of 1.63×10^{14} mol. Consequently, the limiting adsorption of MB corresponds to 35.4% of monolayer coverage.

3.4. Photocatalytic performance

The photonic efficiency ζ is defined as the ratio of the degradation rate and the incident photon flux [34]. It is thus related to the illuminated area and the volume of the employed test solution:

$$\zeta = \frac{V\Delta c}{IAt}$$

with V being the volume, Δc the difference in concentration of the degraded molecule before and after illumination, I the light intensity, A the illuminated area and t is the duration of the illumination.

The emission spectrum of the illumination light source (Osram Eversun) and the absorption spectra of the different dyes are shown in Fig. 8. The maximum irradiation peak of the lamp is in the range of 320–380 nm. Only MO can adsorb UV-light in this area, all other dyes show no UV-screening effect. Also for methyl stearate there is no shielding effect, because there is no absorbance even in the UV-range.

The photonic efficiencies determined for the photocatalytic decomposition of the different dyes differ drastically, ranging from very low values especially for TH to quite reasonable values for MR (Table 2). The photodegradation of methylene blue, which is often used as a reference compound for standard activity tests, on mesoporous films was compared with that measured on the commercial glass Pilkington Active™. The efficiency markedly depends on the thickness of the films, with the thicker T2 film achieving practically the same value as the Pilkington Active™ glass.

The different rate of degradation of MB and TH, both of which are adsorbed on the film surface to a similar extent, can be explained by the degradation mechanism itself. MB is first degraded to TH and subsequently via the intermediates aniline and 4-nitroaniline to acetic acid. Assuming that the photocatalytic degradation of MB to TH is fast and that the subsequent degradation of TH is much slower, this second step will be rate-determining for the overall degradation of MB. For the determination of the photonic efficiency of the degradation of MB, however, only the rate of the first step was measured and not the subsequent decomposition of TH (Fig. 9). Therefore, the photonic efficiency of the degradation of MB is much higher than that of the degradation of TH (Table 2). A reasonable explanation of this phenomenon is that TH might be adsorbed at photocatalytically relative inactive surface sites, while MB possessing additional methyl groups is less adsorbed at these sites

Table 2
Photonic efficiencies (light intensity I = 1 mW/cm^2) of the photocatalytic decomposition of different dye solutions (c = 0.01 mM) on TiO_2 mesoporous films coated at different rates

Sample	ζ_{MB} (%)	ζ_{TH} (%)	ζ_{MR} (%)	ζ_{MO} (%)	ζ_{RB} (%)
Pilkington Active™	0.0236				
T0.5	0.0093	0.0006	0.0311	0.0169	0.0097
T1	0.0190	0.0001	0.0343	0.0214	0.0140
T2	0.0239	0.0012	0.0739	0.0222	0.0360

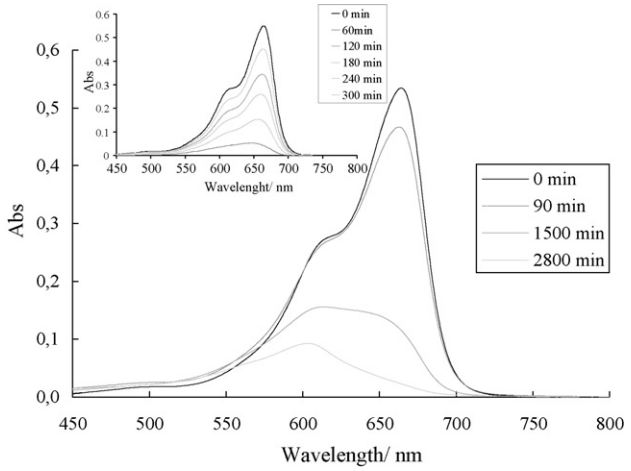

Fig. 9. Absorption spectra showing the photocatalytic degradation of MB (absorption maximum at 664 nm) to TH (absorption maximum around 600 nm) on mesoporous titania film T1. The inserted spectrum shows the photocatalytic degradation of MB on Pilkington Active™ glass.

and is adsorbed at or close to different, photocatalytically more active surface centers. Within the mesoporous structure photocatalytically inactive sites might, for example, be formed during the thermal film preparation step, e.g., by leaving thin carbon layers originating from the structure forming compounds, i.e., the block copolymer, on the surface of a fraction of the titania particles within the pores. Such C-coated titania particles can be considered as excellent adsorption sites while, however, any electron transfer reaction from the bulk to the surface adsorbed species will be blocked efficiently leading to an almost complete recombination of the photogenerated charge carriers. This model is further supported by the following observation. Apparently, the formation of TH as a very stable intermediate in the photocatalytic degradation of MB appears to be a special feature of mesoporous films exhibiting a large surface area. When, for example, the same degradation experiments are carried out employing Pilkington Active™ glass no formation of TH is observed during the spectrophotometric analysis (see inset in Fig. 9). In the latter case, there are apparently no inactive sites where the TH molecules could "hide away" and consequently they are further oxidized as they are formed with no measurable intermediate concentration building up.

The comparison with the other three dyes MR, MO and RB, which are adsorbed to a much lesser extent onto the film's surface while they are photocatalytically degraded with a comparable or even higher efficiency than that observed for MB or TH, evinces that very high surface concentration of the compound to be degraded may even be detrimental. On the one hand, the efficient transfer of holes to molecules adsorbed in multilayers may not be possible. Moreover, intermediates of the parent compound's decomposition also adsorbed on the surfaces may limit the rate of the photocatalytic reaction. Finally, the above described "hide-away" mechanism assuming at least two different classes of adsorption sites, i.e., those with and those without photocatalytic activity, provides a reasonable explanation for such an inverse relationship between adsorption and photonic efficiency. Apparently, an optimum photocatalytic efficiency is achieved when the dye is adsorbed to some extent thus enabling its decomposition directly through the transfer of holes, while, on the other hand, the photocatalytic degradation process might also be initiated in the homogenous solution phase, e.g., as by secondary species such as $O_2^{\bullet -}$ and $HO_2^{\bullet}$.

Table 3
Photonic efficiencies of the photocatalytic decomposition of MB and MR on sample T1 measured repetitively ($I = 1$ mW/cm^2, $c = 0.01$ mM)

Reaction time	ζ_{MB} (%)	ζ_{MR} (%)
Run 1 for 6 h	0.0248	0.0321
Run 2 for 6 h	0.0188	0.0179
Run 3 for 6 h	0.0123	0.0145
Run 4 for 6 h	0.0111	0.0183
Run 5 for 6 h	0.0092	0.0170
Run 6 for 6 h	0.0058	0.0142
Run 7 for 6 h (after regeneration)	0.0190	0.0108

The difference in the degradation mechanism between MB and MR can also be elucidated by the results obtained in long-run experiments. The photonic efficiency of the photodegradation of MB and MR on the film T1 was measured in six subsequent experiments with an illumination time of 360 min each. Hence, the total duration of the illumination was 36 h. In between the single tests the films were stored overnight in the dark immersed in the MB test solution. For the degradation of MB a decrease in the photonic efficiency was observed from one experimental run to the next (Table 3). After regeneration of the film by rinsing with distilled water the photocatalytic activity was increased again (Run 7 in Table 3). It is envisaged that due to the rinsing the degradation products that are blocking parts of the active film surface were removed. As described earlier, the oxidation mechanism of MB involves the splitting-off of CH_3-groups to form TH. Since TH has a much lower solubility in water than MB (2.5 g/L versus 50.0 g/L) and is more strongly adsorbed to the film surface than MB (Fig. 9), this degradation product remains on the film surface thus preventing the adsorption of new intact MB molecules to be degraded. On the contrary, the photonic efficiency of MR decreases only after the first test but remains relatively stable during the following ones, i.e., no systematic deactivation trend is observed. Even after the regeneration no increase in the photonic efficiency is detected. It can be concluded that the active sites on the surface were not blocked by any degradation products and, as already stated above, that a considerable part of the photocatalytic degradation of MR occurs in the homogenous phase most likely initiated by free radical species such as $O_2^{\bullet -}$ and $HO_2^{\bullet}$.

Finally, the efficiency of the mesoporous films for the photocatalytic degradation of methyl stearate in the solid phase was measured. While the photonic efficiency slightly increases with increasing film thickness, being 0.0043 and 0.0059% for the films T 0.5 and T1, respectively, it is found to be considerably lower than that measured for the Pilkington Active™ glass (0.011%). The photonic efficiencies for these solid phase measurements are also considerably lower than the degradation efficiencies of the dyes measured in solution. Apparently, the porous structure of the films can be readily covered with a thin film of the fatty acid methyl stearate; hence, the large surface

area of the films cannot be used efficiently for the decomposition of solid pollutants. Once again, these results suggest that the intermediacy of free radical species such as $O_2^{\bullet -}$, $HO_2^{\bullet}$ and possibly even $OH^{\bullet}$ plays a crucial role in the mode of action of mesoporous photocatalyst films. If their surface is blocked, e.g., through the adsorption of a dye or a fatty acid molecule, the photocatalytic generation of these radicals is hindered and the efficiency decreases dramatically.

4. Conclusions

Mesoporous films of TiO_2 have been shown to be efficient photocatalysts, in particular, for the degradation of dyes, however, this class of materials appears to have both strong and weak features. Their photocatalytic efficiency strongly depends on the respective degradation mechanism. It was found that the optimum efficiency is achieved when the target molecule is adsorbed only to some extent thus enabling its decomposition to be initiated directly by the attack of holes. On the other hand, secondary oxidizing species such as $O_2^{\bullet -}$ and $HO_2^{\bullet}$ but most likely even $OH^{\bullet}$ apparently play a crucial role in the oxidation mechanism which is particularly evident in the case of methylene red. Higher concentrations of adsorbed species to be degraded may even be detrimental as found when thionine was employed as model compound. A novel "hide-away" mechanism is suggested involving two different sites for adsorption with only one of them being photocatalytically active. Consequently, when attempting the degradation of a solid adsorbed layer, the advantageous properties of the mesoporous films cannot be exploited at all and their activity is found to be extremely low. It can, however, be expected that these mesoporous photocatalyst films may be highly effective to initiate photocatalytic degradation processes in the gaseous phase, which is a topic of our current research activities.

Acknowledgement

The authors are grateful to DFG (WA 1116/10 and 436 TSE/130/46/0-1), DAAD (D/04/25758), and the ministry of education, youth and sport of the Czech Republic (1M0577) for the financial support.

References

[1] P. Yang, D. Zhao, D.I. Margolese, B.F. Chmelka, G.D. Stucky, Nature 396 (1998) 152.
[2] C.J. Brinker, Y.F. Lu, A. Sellinger, H.Y. Fan, Adv. Mater. 11 (1999) 579.
[3] D. Grosso, G.J.A.A. Soler-Illia, F. Babonneau, C. Sanchez, P.-A. Albouy, A. Brunet-Bruneau, A.R. Balkenende, Adv. Mater. 13 (2001) 1085.
[4] G.J.A.A. Soler-Illia, A. Louis, C. Sanchez, Chem. Mater. 14 (2002) 750.
[5] E.L. Crepaldi, G.J.A.A. Soler-Illia, D. Grosso, F. Cagnol, F. Ribot, C. Sanchez, J. Am. Chem. Soc. 125 (2003) 9770.
[6] D. Grosso, G.J.D.A. Soler-Illia, E.L. Crepaldi, F. Cagnol, C. Sinturel, A. Bourgeois, A. Brunet-Bruneau, H. Amenitsch, P.A. Albouy, C. Sanchez, Chem. Mater. 15 (2003) 4562.
[7] E.L. Crepaldi, G.J.D.A. Soler-Illia, D. Grosso, F. Cagnol, F. Ribot, C. Sanchez, J. Am. Chem. Soc. 125 (2003) 9770.
[8] K.M. Coakley, Y.X. Liu, M.D. McGehee, K.L. Frindell, G.D. Stucky, Adv. Funct. Mater. 13 (2003) 301.
[9] F. Bosc, A. Ayral, P.A. Albouy, C. Guizard, Chem. Mater. 15 (2003) 2463.
[10] K.L. Frindell, M.H. Bartl, M.R. Robinson, G.C. Bazan, A. Popitsch, G.D. Stucky, J. Solid State Chem. 172 (2003) 81.
[11] B. Smarsly, D. Grosso, T. Brezesinski, N. Pinna, C. Boissiere, M. Antonietti, C. Sanchez, Chem. Mater. 16 (2004) 2948.
[12] Y. Zhang, J. Li, J. Wang, Chem. Mater. 18 (2006) 2917.
[13] M. Wark, J. Tschirch, O. Bartels, D. Bahnemann, J. Rathouský, Micropor. Mesopor. Mater. 84 (2005) 247.
[14] Y. Sakatani, D. Grosso, L. Nicole, C. Boissiere, G. de, A.A. Soler-Illia, C. Sanchez, J. Mater. Chem. 16 (2006) 77.
[15] H. Wang, J.-J. Miao, J.-M. Zhu, H.-M. Ma, J.-J. Zhu, H.-Y. Chen, Langmuir 20 (2004) 11738.
[16] M. Anderson, H. Birkedal, N.R. Franklin, T. Ostomel, S. Boettcher, A.E.C. Palmquist, G.D. Stucky, Chem. Mater. 17 (2005) 1409.
[17] J. Rathouský, D. Fattakhova Rohlfing, M. Wark, T. Brezesinski, B. Smarsly, Thin Solid Films 515 (2007) 6541.
[18] F. Bosc, D. Edwards, N. Keller, V. Keller, A. Ayral, Thin Solid Films 495 (2006) 272.
[19] J.C. Yu, X. Wang, X. Fu, Chem. Mater. 16 (2004) 1523.
[20] J. Tang, Y. Wu, E.W. McFarland, G.D. Stucky, Chem. Commun. 1670. (2004).
[21] X. Wang, J.C. Yu, H.Y. Yip, L. Wu, P.K. Wong, S.Y. Lai, Chem. Eur. J. 11 (2005) 2997.
[22] P.C.A. Alberius, K.L. Frindell, R.C. Hayward, E.J. Kramer, G.D. Stucky, B.F. Chmelka, Chem. Mater. 14 (2002) 3284.
[23] S.K. Lee, A. Mills, Chem. Commun. 18 (2003) 2366.
[24] A. Mills, J.S. Wang, J. Photochem. Photobiol. A 127 (1–3) (1999) 123.
[25] Y. Yang, J. Mol. Catal. A 225 (2005) 203.
[26] M. Stylidi, D.I. Kondarides, X.E. Verykios, Appl. Catal. B 47 (2004) 189.
[27] T. Watanabe, T. Takizawa, K. Honda, J. Phys. Chem. 81 (1977) 1845.
[28] A. Mills, G. Hill, S. Bhopal, I.P. Parkin, S.A. O'Neill, J. Photochem. Photobiol. A 160 (2003) 185.
[29] J. Tschirch, D. Bahnemann, R. Dillert, B. Proft, A. Biedermann, B. Goer, Res. Chem. Intermed., accepted for publication.
[30] P. Jiang, J.F. Bertone, K.S. Hwang, V.L. Colvin, Chem. Mater. 11 (1999) 2132.
[31] C. Kormann, D.W. Bahnemann, M.R. Hoffmann, J. Phys. Chem. 92 (1988) 5196.
[32] R. Comparelli, E. Fanizza, M.L. Curri, P.D. Cozzoli, G. Mascolo, R. Passino, A. Agostiano, Appl. Catal. B Environ. 55 (2005) 81.
[33] P.V. Messina, P.C. Schulz, J. Colloid Interf. Sci. 299 (2006) 305.
[34] S.E. Braslavsky, Pure Appl. Chem. 79 (2007) 293.